Analytical Modelling of No-Load Density in Surface Mounted Permanent Magnet Motor

Frédéric Dubas, Christophe Espanet, A. Miraoui

Analytical Modeling of No-Load Flux Density in Surface Mounted Permanent Magnet Motors

F. Dubas, C. Espanet, *Member*, *IEEE*, and A. Miraoui.
Research Laboratory in Electronics, Electrical engineering and Systems (LEES), which is a joint Research Unit of the University of Technology of Belfort-Monbéliard (UTBM) and the University of Franche-Comté (UFC) with the INRETS (n° LRE-T 31). LEES-UTBM (Bat.F), Rue Thierry MIEG, F90010 Belfort.
E-mail: frederic.dubas@utbm.fr, christophe.espanet@univ-fcomte.fr & abdellatif.miraoui@utbm.fr
Tel: 33 (0)3.84.58.36.29 – Fax: 33 (0)3.84.58.36.36

Abstract

In this paper, the authors present an analytical calculation in order to predict the no-load flux density in surface mounted synchronous permanent magnet machines. This analytical model is based on two-dimensional analysis in polar coordinates and has been developed for both parallel and radial magnetization of the magnets. The no-load magnetic vector potential is established by solving Laplace/Poisson's equations using the Fourier's series and the method of separating variables. Two circular regions are considered: the Region.I, which is the air-gap modified by Carter's coefficient, and the Region.II, which includes the magnets and the air-spaces between magnets. The analytical results are compared with the ones obtained by a numerical analysis using the finite-element method (FEM).

1 Introduction

At the present time, the numerical methods for field computation, such as the finite-elements or the finite-differences, provide accurate results concerning the various magnetic sizes of the electrical machines, with account the saturation etc. But, they are often time-consuming, in particular for three-dimensional models, and don't have the advantage to be sufficiently explicit in comparison with analytical equations. Therefore, several authors proposed two-dimensional analytical models in order to predict the flux density in the synchronous permanent magnet machines [1-7]. Indeed, the accurate knowledge of the magnetic field distribution is a key issue of the performance evaluation of permanent magnet motors, such as demagnetization limit, winding inductances, stator and rotor losses, back-emf, average and cogging torque, forces for the prediction of acoustic noise and vibration spectra, etc. The no-load flux density waveform is mainly affected by number of pole-pairs, air-gap length, magnet configuration (the magnet pole-arc to pole-pitch ratio and the radial thickness of the magnets) and the direction of the magnets magnetization [4]. Thus, in design calculations, it is necessary to study different magnetization patterns (parallel, radial, etc.), possibly including imperfections in the magnetization, for a wide range of magnets shapes. That is why the authors extended their analytical model to account for the tangential magnetization component which can appear at the time of magnet's manufacturing [4-7].

In order to satisfy the continuing request for improving the design's precision and generality, the authors have developed a two-dimensional analytical model in polar coordinates for surface mounted synchronous permanent magnet machines. This model includes both parallel and radial magnetization. It involves the solving Laplace/Poisson's equations using the Fourier's series and the method of separating variables. The results of analytical calculations are compared with the results of numerical simulations carried out by the finite-element method [8].

2 Analytical Model

2.1 Problem Description and Assumptions

The analysis of a surface mounted synchronous permanent magnet machine will be developed for the simplified geometry shown in Fig. 1. The parameters of this geometry are: the inner stator radius modified by Carter's coefficient, R'_s, the outer magnet radius, R_m, the inner magnet radius, R_r, the radial thickness of the magnets, h_m, the air-gap modified by Carter's coefficient, g', the magnet pole-arc to pole-pitch ratio, α_p, the number pole-pairs, p.

The main assumptions are: **1)** End effects are ignored; **2)** The permeability of both stator and rotor steels are assumed infinite, then the saturation effects of the armatures is neglected; **3)** The conductivities of

all regions of the model are assumed to be null; **4)** The permanent magnets are assumed to be nonoriented (with no particular direction of magnetization), isotropic, and having a linear demagnetization characteristic (rare earth magnets); **5)** The slotted stator is transformed into a slotless stator by applying the Carter's coefficient.

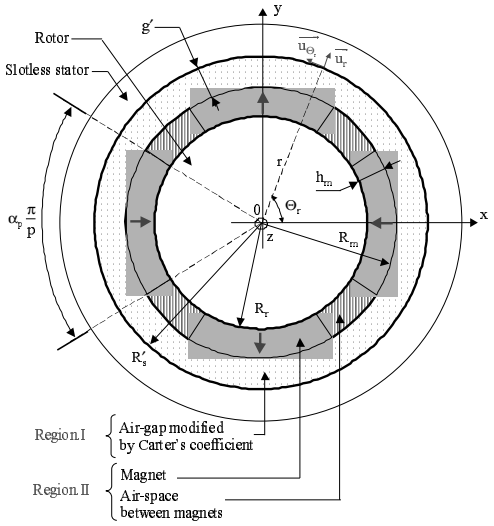

Fig. 1. Simplified motor geometry.

2.2 Modeling of the Magnetization Direction using the Fourier's series

According to the assumptions shown above, in the rare earth magnets (Neodymium-Iron-Boron and Samarium-Cobalt), we can liken the demagnetization characteristic to a linear curve of slope $\mu_0 \cdot \mu_{rm}$ and the flux density equals to the remanent one, B_{rm}, for a magnetic field of 0 A/m. Furthermore, an increase of the operating temperature T_a of the magnet causes a reduction of the remanent flux density and therefore a drop of the demagnetization curve. This influence is quantified using a factor ΔB_{rm} representing the remanent flux density variation of the magnet when the temperature rises 1K [2]:

$$B_{rm}(T_a) = B_{rm0} \cdot \left[1 + \Delta B_{rm} \cdot (T_a - T_{a0})\right] \qquad (1)$$

where T_{a0} is the ambient temperature of the magnet and B_{rm0} is the remanent flux density of the magnet at the temperature T_{a0}.

The remanent flux density vector depends on the direction of the magnets magnetization. Fig. 2 compares parallel and radial magnetization distributions [4]. In polar coordinates, supposing that the magnets are radially homogeneous, the remanent flux density vector is thus given by:

$$\overrightarrow{B^{\mathbf{i}}_{rm}(T_a,\Theta_r)} = B^{\mathbf{ri}}_{rm}(T_a,\Theta_r) \cdot \overrightarrow{u_r} + B^{\mathbf{\Theta i}}_{rm}(T_a,\Theta_r) \cdot \overrightarrow{u_{\Theta_r}} \qquad (2)$$

where $\mathbf{i}$ is the index of the magnetization direction ($\mathbf{i} \Rightarrow$ P: Parallel or $\mathbf{i} \Rightarrow$ R: Radial), Θ_r is the mechanical angular position of the rotor (the position $\Theta_r = 0$ is in the center of a North magnet); $B^{\mathbf{ri}}_{rm}(T_a,\Theta_r)$ and $B^{\mathbf{\Theta i}}_{rm}(T_a,\Theta_r)$ are the radial and tangential components of the remanent flux density vector of the magnet. Fig. 3 shows typical waveforms of these various components, under a pole-pair, according to the direction of the magnets magnetization. Then, $B^{\mathbf{ri}}_{rm}(T_a,\Theta_r)$ and $B^{\mathbf{\Theta i}}_{rm}(T_a,\Theta_r)$ can be expressed as Fourier's series:

$$B^{\mathbf{ri}}_{rm}(T_a,\Theta_r) = \begin{cases} \sum_{n=1,3...}^{+\infty} B^{\mathbf{ri}}_{rm\_n}(T_a,n) \cdot \cos(np \cdot \Theta_r) & p \neq 1 \\ B^{\mathbf{ri}}_{rm\_npl}(T_a) \cdot \cos(\Theta_r) + \sum_{n=3,5...}^{+\infty} B^{\mathbf{ri}}_{rm\_n}(T_a,n) \cdot \cos(np \cdot \Theta_r) & p = 1 \end{cases} \qquad (3.a)$$

$$B^{\mathbf{\Theta i}}_{rm}(T_a,\Theta_r) = \begin{cases} \sum_{n=1,3...}^{+\infty} B^{\mathbf{\Theta i}}_{rm\_n}(T_a,n) \cdot \sin(np \cdot \Theta_r) & p \neq 1 \\ B^{\mathbf{\Theta i}}_{rm\_npl}(T_a) \cdot \sin(\Theta_r) + \sum_{n=3,5...}^{+\infty} B^{\mathbf{\Theta i}}_{rm\_n}(T_a,n) \cdot \sin(np \cdot \Theta_r) & p = 1 \end{cases} \qquad (3.b)$$

where $B^{\mathbf{ri}}_{rm\_n}(T_a,n)$, $B^{\mathbf{\Theta i}}_{rm\_n}(T_a,n)$, $B^{\mathbf{ri}}_{rm\_npl}(T_a)$ and $B^{\mathbf{\Theta i}}_{rm\_npl}(T_a)$ represent the various harmonic amplitudes, for $np \neq 1$ and $np = 1$, of the radial and tangential components for the remanent flux density vector of the magnets. The expressions of these harmonic amplitudes are given in the Appendix 1.

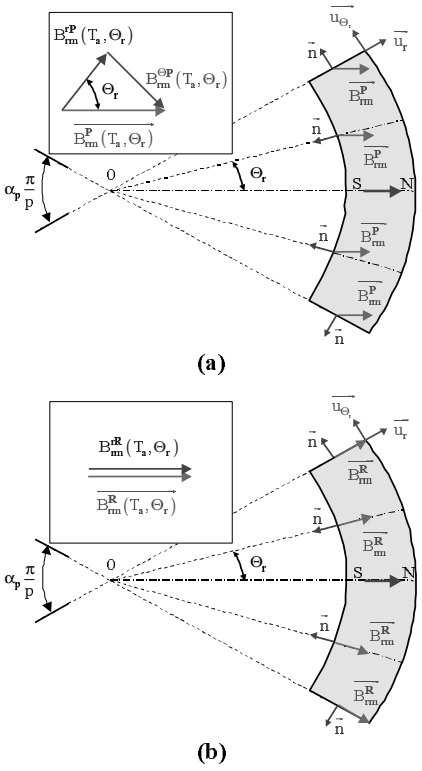

Fig. 2. Direction of the magnets magnetization. **(a)** Parallel magnetization. **(b)** Radial magnetization.

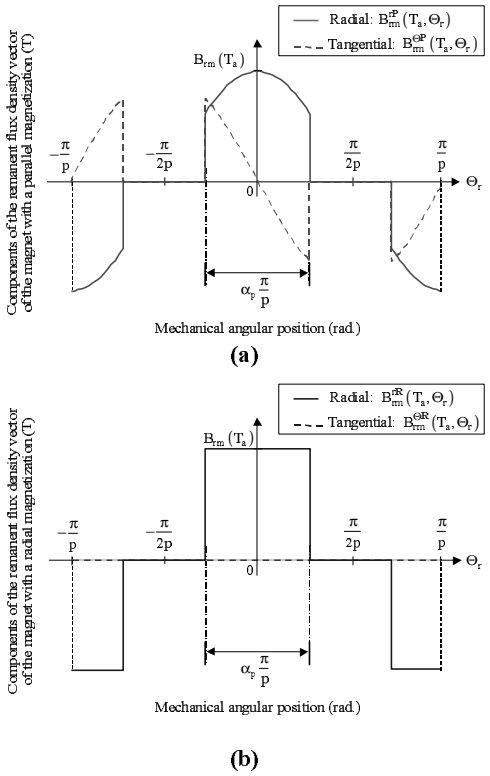

Fig. 3. Waveforms of the radial and tangential components for the remanent flux density vector of the magnet. **(a)** Parallel magnetization. **(b)** Radial magnetization.

2.3 General Equations In Polar Coordinates

2.3.1 General Differential Equations

The Maxwell's equations of magnetostatic are written:

$$\overrightarrow{\mathrm{rot}\left(\vec{H}\right)}=\vec{j} \quad \left(=\vec{0}:\text{No-Load}\right) \qquad \textit{Ampere's law} \qquad (4.a)$$

$$\mathrm{div}\left(\vec{B}\right)=0 \qquad \textit{Magnetic flux conservation} \qquad (4.b)$$

where $\vec{j}$ is the vector of current density, $\vec{H}$ is the magnetic field vector and $\vec{B}$ is the magnetic flux density vector. The magnetic vector potential $\vec{A}$ is defined by:

$$\vec{B}=\overrightarrow{\mathrm{rot}\left(\vec{A}\right)} \quad \text{with} \quad \mathrm{div}\left(\vec{A}\right)=0 \quad \textit{Coulomb's gage} \qquad (4.c)$$

$\vec{B}$ and $\vec{H}$ verify the magnetic material equation:

$$\vec{B}=f\left(\vec{H}\right) \qquad (5)$$

where the function f is dependent on the material physical properties.

The domain of study consists in four circular regions (Fig. 1): the slotless stator, the air-gap modified by the Carter's coefficient (**Region.I**), the region including the magnets and the air-spaces between magnets (**Region.II**) and finally the rotor. According to the working assumptions, the magnetic field of the slotless stator and the rotor can be considered as null. Therefore, the domain of study is reduced to two circular regions:

- **Region.I: $R_m \le r \le R'_s$:**

$$\overrightarrow{B_{Iv}}=\mu_0\cdot\overrightarrow{H_{Iv}} \qquad (6)$$

- **Region.II: $R_r \le r \le R_m$:**

$$\overrightarrow{B^{i}_{IIv}}=\mu_0\cdot\mu_{rII}\left(\Theta_r\right)\cdot\overrightarrow{H^{i}_{IIv}}+\overrightarrow{B^{i}_{rm}\left(T_a,\Theta_r\right)} \qquad (7)$$

where μ_0 is the permeability of free space, $\mu_{rII}\left(\Theta_r\right)$ is the relative magnetic permeability of Region.II. We can remark, on the Fig. 1, that $\mu_{rII}\left(\Theta_r\right)$ is not constant: $\mu_{rII}=1$ in the air-space between magnets and $\mu_{rII}=\mu_{rm}$ in the magnets.

Using equations (4), (6) and (7), and neglecting the end effects ($\overrightarrow{\Delta A_v} = A_v^z \cdot \overrightarrow{u_z}$), the no-load magnetic vector potential, in each region, verifies the following equations:

$$\Delta A_{Iv}^{zi} = 0 \qquad (8.a)$$

$$\frac{1}{r^2} \cdot \frac{\partial \mathbf{a}(\Theta_r)}{\partial \Theta_r} \cdot \frac{\partial A_{IIv}^{zi}}{\partial \Theta_r} + \mathbf{a}(\Theta_r) \cdot \Delta A_{IIv}^{zi} = \frac{1}{r} \cdot \mathbf{b}(T_a, \Theta_r) \qquad (8.b)$$

where the functions $\mathbf{a}(\Theta_r)$ and $\mathbf{b}(T_a, \Theta_r)$ are given in the Appendix 2.

2.3.2 *The Assumption of Relative Magnetic Permeability Homogeneity in Region.II*

To solve the differential equations above, we use the method of separating variables. The equation (8.a) is classical, contrary to (8.b) which results in solving a second-order differential equation with no-constant coefficients. To eliminate this problem, the rotor is transformed into an equivalent one, where the relative magnetic permeability of Region.II is supposed constant ($\mu_{rII}(\Theta_r) = \mu_{rII}$). Contrary to [7], we suppose that μ_{rII} equals to 1 and we correct the remanent flux density of the magnet, $B_{rm}(T_a)$, to minimize the error of computation [2], [4]:

$$B_{rmc}(T_a) = k_m \cdot B_{rm}(T_a) = \frac{1 + \mu_{rm}}{2 \cdot \mu_{rm}} \cdot B_{rm}(T_a) \qquad (9)$$

where B_{rmc} is the corrected remanent flux density at the temperature T_a and μ_{rm} is the relative magnetic permeability of the magnet. We remark that for $\mu_{rm} = 1.2$, the maximum error $\varepsilon_{B_{rm}} = 1 - k_m$ on the remanent flux density equals to 8.33%.

By applying the assumption of relative magnetic permeability homogeneity in Region.II and by using the equation (8.b), the no-load magnetic vector potential in Region.II verifies the following equation:

$$\Delta A_{IIv}^{zi} = -\frac{1}{r} \cdot \left[B_{rmc}^{\Theta i}(T_a, \Theta_r) - \frac{\partial B_{rmc}^{ri}(T_a, \Theta_r)}{\partial \Theta_r} \right] \qquad (10)$$

2.4 General Solutions In Polar Coordinates

The boundary conditions in the two regions are defined by:

$$B_{Iv}^{\Theta i}(R'_s, \Theta_r) = 0 \qquad (11.a)$$

$$B_{Iv}^{\Theta i}(R_m, \Theta_r) = B_{IIv}^{\Theta i}(R_m, \Theta_r) - B_{rmc}^{\Theta i}(T_a, \Theta_r) \qquad (11.b)$$

$$B_{Iv}^{ri}(R_m, \Theta_r) = B_{IIv}^{ri}(R_m, \Theta_r) \qquad (11.c)$$

$$B_{IIv}^{\Theta i}(R_r, \Theta_r) = B_{rmc}^{\Theta i}(T_a, \Theta_r) \qquad (11.d)$$

By solving the equations (8.a) and (10) with the equations (11), the Fourier's series of the no-load vector magnetic potential can be obtained. In each region, the curl of the no-load magnetic vector potential, (4.c), gives the radial and tangential components of no-load flux density vector:

$$B_{jv}^{ri}(T_a, r, \Theta_r) = \begin{cases} -\sum_{n=1,3...}^{+\infty} B_{jv\_n}^{ri}(T_a, r, n) \cdot \cos(np \cdot \Theta_r) & p \neq 1 \\ B_{jv\_np1}^{ri}(T_a, r) \cdot \cos(\Theta_r) - \sum_{n=3,5...}^{+\infty} B_{jv\_n}^{ri}(T_a, r, n) \cdot \cos(np \cdot \Theta_r) & p = 1 \end{cases} \qquad (12.a)$$

$$B_{jv}^{\Theta i}(T_a, r, \Theta_r) = \begin{cases} -\sum_{n=1,3...}^{+\infty} B_{jv\_n}^{\Theta i}(r, n) \cdot \sin(np \cdot \Theta_r) & p \neq 1 \\ B_{jv\_np1}^{\Theta i}(T_a, r) \cdot \sin(\Theta_r) - \sum_{n=3,5...}^{+\infty} B_{jv\_n}^{\Theta i}(T_a, r, n) \cdot \sin(np \cdot \Theta_r) & p = 1 \end{cases} \qquad (12.b)$$

where **j** is the index of the region ($\mathbf{j} \Rightarrow I$: Region.I or $\mathbf{j} \Rightarrow II$: Region.II) ; $B_{jv\_n}^{ri}(T_a, r, n)$, $B_{jv\_n}^{\Theta i}(T_a, r, n)$, $B_{jv\_np1}^{ri}(T_a, r)$ and $B_{jv\_np1}^{\Theta i}(T_a, r)$ represent the various harmonic amplitudes, in each region, for $np \neq 1$ and $np = 1$ of the radial and tangential components for the no-load flux density vector. The expressions of these harmonic amplitudes are given in the Appendix 3.

3 Comparison with the Finite-Element Calculations

The developed model has been applied to a three-phase, slotless permanent magnet brushless motor with an internal rotor and either parallel or radial magnetized magnets. For the analytical-numerical comparison, the geometric sizes of the motor and the physical parameters of the magnet are: $R'_s = 20$ mm, $R_m = 19$ mm, $R_r = 16$ mm, $p = 1$, $B_{r0} = 1.08$ T for $T_{a0} = 20$ °C, $\Delta B_r = -0.12$ %/K and $\mu_{rm} = 1.029$ (Neodymium-Iron-Boron: *N30H*).

Figs. 4 and 5 show excellent agreement between analytical and finite-element predicted distributions of the components of no-load flux density. This is true, in each region, for both parallel and radial magnetization and for $\alpha_p = 1$ or $\alpha_p = 0.8$.

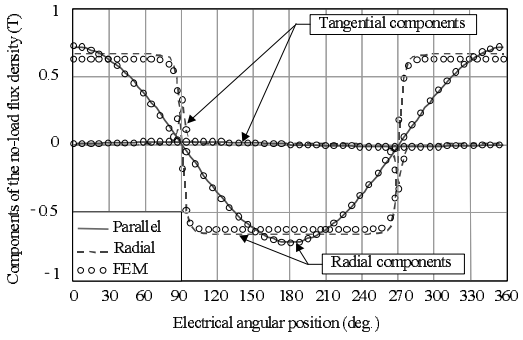

Fig. 4. Distribution of the radial and tangential components with a parallel or radial magnetization at T_a = 100 °C for α_p = 1. **(a)** Region.I (r = 19.5 mm). **(b)** Region.II (r = 17.5 mm).

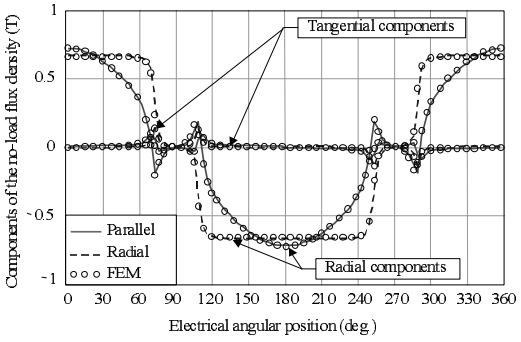

Fig. 5. Distribution of the radial and tangential components with a parallel or radial magnetization at T_a = 100 °C for α_p = 0.8. **(a)** Region.I (r = 19.5 mm). **(b)** Region.II (r = 17.5 mm).

4 Conclusion

A two-dimensional analytical model in polar coordinates has been developed for surface mounted synchronous permanent magnet machines. This model makes it possible to determine the no-load flux density created by the magnets in Region.I (the air-gap modified by the Carter's coefficient) and Region.II (the region including the magnets and the air-spaces between magnets). To improve the design's precision and generality, the authors have introduced into the analytical model the choice between two types of magnets magnetization: Parallel or Radial. The agreement of the results of analytical and numerical calculations is quite good. The maximum error for the comparison analytical-numerical is 1.41%, which is reasonable for a analytical model. This error is primarily due to the assumption of relative magnetic permeability homogeneity in Region.II.

References

[1] Z.Q. Zhu, D. Howe, E. Bolte and B. Ackermann – "Instantaneous Magnetic Filed Distribution in Brushless Permanent Magnet dc Motors, Part I :

Open-Circuit Field", **IEEE Transactions on Magnetics**, Vol.29, No.1, January 1993, pp.124-135.

[2] C. Espanet – "Modélisation et conception optimale de moteurs sans balais à structure inversée. Application au moteur-roue", **Thesis**, University of Franche-Comté (UFC), Belfort, January 1999, pp.153-165 and pp.273-275.

[3] M. Markovic, M. Jufer and A. Cassat – "A modulation method to determine the magnetic field in PM motors", **Electrimacs**, August 2002, pp.1-6.

[4] N. Boules – "Prediction of No-Load Flux Density Distribution in Permanent Magnet Machines", **IEEE Transaction on Industry Applications**, Vol.IA-21, No.4, May/June 1985, pp.633-643.

[5] K.F. Rasmussen – "Analytical Prediction of Magnetic Field from Surface Mounted Permanent Magnet Motor", **in Proc IEEE Electrical Machines and Drives Conf.**, Seattle, WA, May 1999, pp.34-36.

[6] K.F. Rasmussen, J.H. Davies, T.J.E Miller, M.I. McGilp and M. Olaru – "Analytical and Numerical Computation of Air-Gap Magnetic Fields in Brushless Motors with Surface Permanent Magnets", **IEEE Transactions on Industry Applications**, Vol.36, No.6, November/December 2000, pp.1547-1554.

[7] Z.Q. Zhu, D. Howe and C.C. Chan – "Improved Analytical Model for Predicting the Magnetic Field Distribution in Brushless Permanent Magnet Machines", **IEEE Transactions on Magnetics**, Vol.38, No.1, January 2002, pp.229-238.

[8] FLUX2D – "Notice d'utilisation générale", Version 7.50. Cedrat S.A Electrical Engineering, 10 Chemin de pré carré, Zirst, 38246 MEYLAN Cedex-FRANCE.

Appendix

Appendix 1: The different harmonic amplitudes; for $np \neq 1$, $np = 1$ and parallel or radial magnetization; of the radial and tangential components for the remanent flux density vector of the magnets are:

✓ ***the harmonic amplitudes of the radial component:***

$$B_{rm\_n}^{rP}(T_a, n) = \frac{2p \cdot B_{rm}(T_a)}{\pi\left[1-(np)^2\right]} \cdot \left\{(1-np)\cdot \sin\left[(1+np)\cdot \alpha_p \frac{\pi}{2p}\right] + (1+np)\cdot \sin\left[(1-np)\cdot \alpha_p \frac{\pi}{2p}\right]\right\} \quad \text{(A1.a)}$$

$$B_{rm\_np1}^{rP}(T_a) = \frac{B_{rm}(T_a)}{\pi} \cdot \left[\sin(\alpha_p \pi) + \alpha_p \pi\right] \quad \text{(A1.b)}$$

$$B_{rm\_n}^{rR}(T_a, n) = \frac{4 \cdot B_{rm}(T_a)}{n\pi} \cdot \sin\left[n\alpha_p \frac{\pi}{2}\right] \quad \text{(A1.c)}$$

$$B_{rm\_np1}^{rR}(T_a, n) = \frac{4 \cdot B_{rm}(T_a)}{\pi} \cdot \sin\left[\alpha_p \frac{\pi}{2}\right] \quad \text{(A1.d)}$$

✓ ***the harmonic amplitudes of the tangential component:***

$$B_{rm\_n}^{\Theta P}(T_a, n) = \frac{2p \cdot B_{rm}(T_a)}{\pi\left[1-(np)^2\right]} \cdot \left\{(1-np)\cdot \sin\left[(1+np)\cdot \alpha_p \frac{\pi}{2p}\right] - (1+np)\cdot \sin\left[(1-np)\cdot \alpha_p \frac{\pi}{2p}\right]\right\} \quad \text{(A1.e)}$$

$$B_{rm\_np1}^{\Theta P}(T_a) = \frac{B_{rm}(T_a)}{\pi} \cdot \left[\sin(\alpha_p \pi) - \alpha_p \pi\right] \quad \text{(A1.f)}$$

$$B_{rm\_n}^{\Theta R}(T_a, n) = 0 \quad \text{(A1.g)}$$

$$B_{rm\_np1}^{\Theta R}(T_a) = 0 \quad \text{(A1.h)}$$

Appendix 2:

$$\mathbf{a}(\Theta_r)=\frac{1}{\mu_0\cdot\mu_{rII}(\Theta_r)} \tag{A2.a}$$

$$\mathbf{b}(T_a,r,\Theta_r)=\frac{\partial\mathbf{a}(\Theta_r)}{\partial\Theta_r}\cdot B_{rm}^{ri}(T_a,\Theta_r)-\mathbf{a}(\Theta_r)\cdot\left[B_{rm}^{\Theta i}(T_a,\Theta_r)-\frac{\partial B_{rm}^{ri}(T_a,\Theta_r)}{\partial\Theta_r}\right] \tag{A2.b}$$

Appendix 3: The different harmonic amplitudes, in each region, for $np\neq 1$ and $np=1$ of the radial and tangential components for the no-load flux density vector are:

- **in Region.I: $R_m \le r \le R'_s$:**

  - ✓ ***the harmonic amplitudes of the radial component:***

$$B_{Iv\_n}^{ri}(T_a,r,n)=B_{Iv\_n}^{i}(T_a,n)\cdot\left[\left(\frac{R_m}{R'_s}\right)^{np}\left(\frac{r}{R'_s}\right)^{np}+\left(\frac{R_m}{r}\right)^{np}\right]\cdot\frac{R_m}{r} \tag{A3.a}$$

$$B_{Iv\_npl}^{ri}(T_a,r)=B_{Iv\_npl}^{i}(T_a)\cdot\left[1+\left(\frac{R'_s}{r}\right)^{2}\right] \tag{A3.b}$$

  - ✓ ***the harmonic amplitudes of the tangential component:***

$$B_{Iv\_n}^{\Theta i}(T_a,r,n)=B_{Iv\_n}^{i}(T_a,n)\cdot\left[\left(\frac{R_m}{r}\right)^{np}-\left(\frac{R_m}{R'_s}\right)^{np}\left(\frac{r}{R'_s}\right)^{np}\right]\cdot\frac{R_m}{r} \tag{A3.c}$$

$$B_{Iv\_npl}^{\Theta i}(T_a,r)=B_{Iv\_npl}^{i}(T_a)\cdot\left[\left(\frac{R'_s}{r}\right)^{2}-1\right] \tag{A3.d}$$

- **in Region.II: $R_r \le r \le R_m$:**

  - ✓ ***the harmonic amplitudes of the radial component:***

$$B_{IIv\_n}^{ri}(T_a,r,n)=B_{IIv\_n}^{i}(T_a,n)\cdot\left[\left(\frac{r}{R_m}\right)^{np-1}+\left(\frac{R_r}{R_m}\right)^{np-1}\left(\frac{R_r}{r}\right)^{np+1}\right]+\mathbf{e}^{i}(T_a,n)\cdot\left(\frac{R_r}{r}\right)^{np+1}+np\cdot\mathbf{c}^{i}(T_a,n) \tag{A3.e}$$

$$B_{IIv\_npl}^{ri}(T_a,r)=B_{IIv\_npl}^{i}(T_a)\cdot\left[1+\left(\frac{R_r}{r}\right)^{2}\right]+\frac{\mathbf{d}^{i}(T_a)}{2}\cdot\left[1-\ln\left(\frac{r}{R_m}\right)+\left(\frac{R_r}{r}\right)^{2}\ln\left(\frac{R_m}{R_r}\right)\right]-B_{rmc\_npl}^{\Theta i}(T_a) \tag{A3.f}$$

  - ✓ ***the harmonic amplitudes of the tangential component:***

$$B_{IIv\_n}^{\Theta i}(T_a,r,n)=B_{IIv\_n}^{i}(T_a,n)\cdot\left[\left(\frac{R_r}{R_m}\right)^{np-1}\left(\frac{R_r}{r}\right)^{np+1}-\left(\frac{r}{R_m}\right)^{np-1}\right]+\mathbf{e}^{i}(T_a,n)\cdot\left(\frac{R_r}{r}\right)^{np+1}-\mathbf{c}^{i}(T_a,n) \tag{A3.g}$$

$$B_{IIv\_npl}^{\Theta i}(T_a,r)=B_{IIv\_npl}^{i}(T_a)\cdot\left[\left(\frac{R_r}{r}\right)^{2}-1\right]+\frac{\mathbf{d}^{i}(T_a)}{2}\cdot\left[\ln\left(\frac{r}{R_m}\right)+\left(\frac{R_r}{r}\right)^{2}\ln\left(\frac{R_m}{R_r}\right)\right]+B_{rmc\_npl}^{\Theta i}(T_a) \tag{A3.h}$$

where:

$$B^{i}_{Iv\_n}(T_a,n)=\frac{\left[2\cdot \mathbf{e}^{i}(T_a,n)\cdot\left(\frac{R_r}{R_m}\right)^{np+1}+\mathbf{f}^{i}(T_a,n)\cdot\left(\frac{R_r}{R_m}\right)^{2np}+\mathbf{g}^{i}(T_a,n)\right]}{2\cdot\left[1-\left(\frac{R_r}{R'_s}\right)^{2np}\right]} \tag{A3.i}$$

$$B^{i}_{Iv\_npl}(T_a)=\frac{\left[\frac{\mathbf{d}^{i}(T_a)}{2}-B^{\Theta i}_{rmc\_npl}(T_a)\right]\cdot\left[\left(\frac{R_m}{R'_s}\right)^{2}-\left(\frac{R_r}{R'_s}\right)^{2}\right]+\mathbf{d}^{i}(T_a)\cdot\left(\frac{R_r}{R'_s}\right)^{2}\ln\left(\frac{R_m}{R_r}\right)}{2\cdot\left[1-\left(\frac{R_r}{R'_s}\right)^{2}\right]} \tag{A3.j}$$

$$B^{i}_{IIv\_n}(T_a,n)=\frac{\left[2\cdot \mathbf{e}^{i}(T_a,n)\cdot\left(\frac{R_r}{R'_s}\right)^{np+1}\left(\frac{R_m}{R'_s}\right)^{np-1}+\mathbf{f}^{i}(T_a,n)+\mathbf{g}^{i}(T_a,n)\cdot\left(\frac{R_m}{R'_s}\right)^{2np}\right]}{2\cdot\left[1-\left(\frac{R_r}{R'_s}\right)^{2np}\right]} \tag{A3.k}$$

$$B^{i}_{IIv\_npl}(T_a)=\frac{\left[\frac{\mathbf{d}^{i}(T_a)}{2}-B^{\Theta i}_{rmc\_npl}(T_a)\right]\cdot\left[\left(\frac{R_m}{R'_s}\right)^{2}-1\right]+\mathbf{d}^{i}(T_a)\cdot\left(\frac{R_r}{R'_s}\right)^{2}\ln\left(\frac{R_m}{R_r}\right)}{2\cdot\left[1-\left(\frac{R_r}{R'_s}\right)^{2}\right]} \tag{A3.l}$$

$$\mathbf{e}^{i}(T_a,n)=\mathbf{c}^{i}(T_a,n)-B^{\Theta i}_{rmc\_n}(T_a,n) \tag{A3.m}$$

$$\mathbf{f}^{i}(T_a,n)=B^{\Theta i}_{rmc\_n}(T_a,n)-(np+1)\cdot\mathbf{c}^{i}(T_a,n) \tag{A3.n}$$

$$\mathbf{g}^{i}(T_a,n)=B^{\Theta i}_{rmc\_n}(T_a,n)+(np-1)\cdot\mathbf{c}^{i}(T_a,n) \tag{A3.o}$$

$$\mathbf{c}^{i}(T_a,n)=\frac{B^{\Theta i}_{rmc\_n}(T_a,n)+np\cdot B^{ri}_{rmc\_n}(T_a,n)}{\left[1-(np)^{2}\right]} \tag{A3.p}$$

$$\mathbf{d}^{i}(T_a)=B^{\Theta i}_{rmc\_npl}(T_a)+B^{ri}_{rmc\_npl}(T_a) \tag{A3.q}$$